INTERNATIONAL JOURNAL FOR NUMERICAL AND ANALYTICAL METHODS IN GEOMECHANICS
Int. J. Numer. Anal. Meth. Geomech., **23**, 1427–1454 (1999)

AN ANALYSIS OF GEOTECHNICAL PROBLEMS INVOLVING STRAIN SOFTENING EFFECTS

DONATELLA STERPI

Department of Structural Engineering, Politecnico di Milano, P. Leonardo da Vinci 32-20133, Milano, Italy

SUMMARY

The phenomenon of strain localization and the associated softening effects are here approached from a macroscopic viewpoint. A finite element model is proposed which includes two possible aspects of the phenomenon. The first one, referred to as 'structural softening', leads to a criterion for detecting the onset of localization which depends on the current values of the stress components. A simple analytical example is discussed which shows how this approach can lead to strain softening even for elastic perfectly plastic materials, in the presence of a non-associated flow rule. The second approach to the phenomenon, referred to as 'material softening', assumes that the initiation of softening depends on the accumulated plastic strains. Some applications of these approaches are discussed, concerning the situation of small-scale model tests on shallow tunnels. On the basis of the comparison between experimental and numerical results some comments are presented on the effectiveness of the procedure in capturing the collapse mechanism of the opening. Copyright © 1999 John Wiley & Sons, Ltd.

KEY WORDS: strain localization; shear band analysis; strain softening; small-scale model; tunnelling

1. INTRODUCTION

In geotechnical engineering the term 'strain softening' is customarily adopted for denoting materials such as rocks, dense sands or overconsolidated clays that, when subjected for instance to a compression test, show a loss of their overall load-carrying capacity with increasing deformation, after a peak load level has been reached. Quite often this behaviour is associated to the formation of zones of limited thickness within the sample where irreversible strains localize, eventually leading to failure through the formation of a collapse mechanism.

When dealing with large-scale engineering problems, this phenomenon and the associated loss of the overall resistance of the soil/rock mass, is considered as one of the main causes of the so-called 'progressive failure' of slopes and underground openings.[1–3]

The possible onset of zones of localization during laboratory tests, as well as their geometrical characteristics, such as orientation and thickness, are strongly influenced by the nature and state of the material and by the testing conditions. Depending on the material characteristics, two different modes of localization can be observed. The first one is typical of material having an appreciable cohesion (e.g. rocks) and leads to the formation of fractures along which the cohesive component of the shear resistance vanishes. The second mode characterizes frictional materials

* Correspondence to: D. Sterpi, Department of Structural Engineering, Politecnico di Milano, P. Leonardo da Vinci 32-20133, Milano, Italy

CCC 0363–9061/99/131427–28$17.50
Copyright © 1999 John Wiley & Sons, Ltd.
Received 26 March 1998
Revised 17 August 1998

(e.g. dense sands) and leads to the formation of narrow shear bands within which the structure of the granular material undergoes a marked change. In particular, a decrease of its relative density takes place, with a consequent substantial reduction of its frictional resistance.

In both cases, the process of localization should be studied considering separately the condition governing its onset and the process of spread and coalescence of the zones of localization, until a continuous failure surface is originated.

The study of this complex phenomenon, which includes the mode of localization (by fracturing or by shear banding) and the rules governing its onset and spread, has been approached in the literature considering both 'micro-mechanical' and 'macroscopic' viewpoints. In the first case, the phenomenon is analysed by directly modelling the interaction between the granular particles[4,5] or the crystal grains of the material.[6] The macroscopic approach attempts to model the overall behaviour of the strain softening material on the basis of the results of large scale (with respect to the size of the soil/rock particles) laboratory tests and of field observations, without going into the details of the interaction between its microscopic components. Even though this second approach presents some drawbacks with respect to the micro-mechanical approach, it seems preferable for deriving global behaviour models applicable to the analysis of large-scale engineering problems, and will be followed in the present study. The discussion will be limited to the case of shear band formation and spreading, considering in particular frictional and moderately cohesive soils or weak rocks.

In the following, two alternative hypotheses on the causes of softening initiation will be first discussed. The first one, referred to as 'material' or intrinsic softening, considers the loss of the load-carrying capacity as an intrinsic property of the material, introduced at the constitutive law level, that might in turn cause the formation of shear bands. In the second case, referred to as 'structural' softening, the onset of the phenomenon is related to the fulfilment of a local bifurcation condition on the system of solving equations for the boundary value problem. According to this approach, which is conceptually similar to that used for evaluating the critical load of compressed truss, the onset of softening is not necessarily related to a loss of shear resistance introduced in the chosen stress–strain law.

Subsequently, after discussing the analytical solution of a simple 'structural' softening problem for a cohesionless material, a finite element approach for softening analysis is illustrated which includes both 'material' and 'structural' viewpoints. Finally, the proposed approach is applied to the solution of some significant bench mark problems, comparing the numerical results with available experimental data.

Notation. A matrix notation is used herein to describe the numerical solution approach. Boldface, uppercase and lowercase letters denote matrices and column vectors, respectively. A superposed dot indicates infinitesimal increments and a superscript T means transpose.

2. 'MATERIAL' AND 'STRUCTURAL' SOFTENING

2.1. *Material softening*

Following the 'material', or intrinsic, approach to softening, the loss of the overall bearing capacity observed, for instance, during a compression test on a sample of dense sand is considered as a direct consequence of the material behaviour, which shows a reduction of the shear strength with increasing deformation.[7–9] This reduction initiates when a given condition on the strain state is attained. In other words, it is assumed that strain softening

Copyright © 1999 John Wiley & Sons, Ltd.

is an intrinsic characteristic of the constitutive law which presents a descending branch of the stress–strain diagram. This, in turn, implies local instability of the material,[10] since along this descending branch the increments of stresses and strains, respectively grouped in vectors $\dot{\boldsymbol{\sigma}}$ and $\dot{\boldsymbol{\varepsilon}}$, satisfy the condition

$$\dot{\boldsymbol{\varepsilon}}^{\mathrm{T}}\dot{\boldsymbol{\sigma}} < 0 \tag{1}$$

The above local condition can progressively lead to irreversible strain localization, and eventually to global instability.

It should be considered, however, that when this kind of behaviour is introduced in a standard time-independent constitutive model some physically meaningless consequences arise for both initial and boundary value problems.[11] In particular, a change in the characteristic of the solving equations system is produced, which causes the ill-posedness of the formulation.

When solved by means of numerical (e.g. finite element) methods, an ill-posed problem generally shows numerical instability and dependence of the solution from the discretization. In the case of localization problems, the mesh dependence affects both the computed thickness of the shear band, that decreases with decreasing element size, and its direction, that easily follows the alignment of the element sides.[12,13]

It should also be considered that the derivation of the constitutive law, defined on an infinitesimal volume, from the behaviour observed during laboratory tests on samples having a finite volume, requires the assumption of homogeneity of the stress and strain fields within the sample. However, due to the formation of shear bands, this homogeneity is in general lost in the descending branch of the measured load–displacement diagram. In particular, the assumed reacting area of the specimen might be overestimated, leading to the underestimation of the current stresses. As a limit case, the real stress–strain diagram does not show any descending branch if the rate of decrease of the actual reacting area is larger than the one of the applied load.[14]

2.2. Structural softening

An alternative way to solve strain softening problems is offered by the 'structural' approach. This rests on the assumption that in a numerical analysis the macroscopic phenomenon of strain softening initiates when the uniqueness of solution of the solving equation system for the problem under consideration is lost, regardless the particular constitutive model adopted in the calculations.

For a given material element, a point of bifurcation is first sought along the load–displacement path where, for an increment of external actions, alternative solutions of the governing equations exist different from the trivial one. Among them, the particular solution is searched for that exhibits the non homogeneities in the strain field similar to those experimentally observed, i.e. shear bands. This requires to carry out a 'shear band analysis', in the framework of the bifurcation theory, at each step of the loading process and for each point of the continuum, in order to find out the non-trivial solution which includes a discontinuity in the strain field, locally represented by a plane. The consequent criterion for softening initiation depends on the current values of the stress components.

The characteristics of the material model play a main role in the bifurcation analysis. It has been shown, in fact, that the loading path bifurcation is possible for ideally plastic or positive hardening materials, provided that the plastic flow rule is non associated,[15,16] whereas in the

Copyright © 1999 John Wiley & Sons, Ltd.

presence of an associated flow rule bifurcation can occur only in the case of negative hardening, that drives back to the intrinsic softening previously considered.

Note that the mentioned bifurcation analysis provides only the directions of the possible shear bands, if any, and the location of the points where they initiate. Consequently, a suitable post-bifurcation procedure has to be introduced in the calculations in order to follow the actual alternative path beyond the bifurcation point.[17]

3. SOME *AD HOC* TECHNIQUES FOR SOFTENING ANALYSIS BY FINITE ELEMENTS

When a problem involving strain softening behaviour is studied by a numerical approach, e.g. by the finite element method, some difficulties might arise, related to inception and development of localization and to the above-mentioned mesh dependence. To overcome or limit these drawbacks various strategies have been proposed in the literature.

Some of these, referred to as 'regularization techniques', allow to avoid mesh dependence of the solution by introducing a characteristic internal length, related to the microstructure of the material, into the physical formulation of the problem. In fact, these techniques are mainly based on non-conventional definitions of the continuum, such as those involving Cosserat continuum,[18–20] or on particular constitutive models. Among these, the non-local constitutive models introduce the internal length by averaging stresses and strains, or related variables, on a finite material volume,[11,21,22] while the gradient-dependent models[23] add higher-order terms of the strain gradient into the constitutive relationships.[24–26] Comparison[27] and integration[28,29] of these models with Cosserat continuum have been also presented. Other techniques introduce the strain rate sensitivity in the constitutive law, through a fictitious viscosity, which again leads to the definition of a characteristic length of the material.[30,31] A notable approach to non-linear and time-dependent material problems is represented by the model based on the Disturbed State Concept.[32–34] In this model, the material undergoing deformation is considered to 'self-adjust' between two limit states (i.e. the relative intact and the fully adjusted states), the behaviour of which is characterized by independent constitutive laws. In particular, this approach is able to account for softening effects without requiring the use of *ad hoc* assumption on particular continua.

Alternative provisions have been also proposed which directly concern the features of the numerical model. They enable the analysis to capture zones of high strain concentration, as well as to follow the progress of shear bands, trying to overcome the limit represented by the continuity and derivability of the displacement functions of standard elements. Some of them suggest the use of a biased finite element discretization, obtained by aligning the sides of the elements along the expected direction of the shear bands, which can be estimated by a preliminary shear band analysis.[12] Also a discretization with crossed triangular elements, formed by subdividing adjacent quadrilateral elements into four triangles through their diagonals, allows for a richer pattern of possible shear band directions.[35] The difficulty in capturing zones of high strain concentration could be reduced by resorting to adaptive remeshing techniques, which permit a gradual refinement of the grids in those zones where the concentration of strains is detected.[36,37] Alternatively, the use of special elements has been proposed in order to model the occurrence of a discontinuity plane within the elements. In some cases the standard shape functions are enriched with particular functions able to model a displacement discontinuity, the characteristics of which are defined through a shear band analysis.[38–40] In other cases the

Copyright © 1999 John Wiley & Sons, Ltd.

enrichment of the element deformation is obtained by including an embedded shear layer within it, representing the band of strain localization.[41,42]

An easier procedure to follow the post bifurcation path, that avoids the non-negligible programming effort required by some of the above provisions, is based on the use of a non-isotropic material law. For the elements were localization is detected the initially homogeneous material is substituted by a 'structured' composite material, having average mechanical properties determined through homogenization, so that the effect of the band crossing the element is smeared all over it.[43–45]

It should also be mentioned that, in order to inhibit the tendency of ordinary finite element analyses to overlook the onset of bifurcation and to lead to the trivial homogeneous solution, the bifurcated path can be forced by introducing artificial non-homogeneities or 'trigger' elements in the mesh.[46,47]

Further details on the various numerical procedures for strain localization analysis can be found, e.g. in References 48–52.

4. AN ANALYTICAL EXAMPLE OF STRUCTURAL SOFTENING

To clarify the bases of the 'structural' approach, the analytical solution of a simple problem is discussed in which softening shows up in an elastic-prefectly plastic material obeying a non-associated flow rule.

To this purpose consider a two-dimensional element, in a Cartesian reference system x_1, x_2, in plane strain conditions. The element consists of a purely frictional material obeying an elastic-perfectly plastic constitutive law with Drucker–Prager yield criterion that, assuming the compressive stresses as positive, is expressed by the following equation:

$$F = \sqrt{J_2} - \alpha I_1 = 0 \tag{2}$$

Here I_1 and J_2 are the first stress invariant and the second invariant of the deviatoric stresses, respectively, and α is a material parameter depending on the friction angle.

The element is subjected to an initial stress state, denoted by suffix A, having the following components:

$$\sigma_{1A} = \sigma_0, \quad \sigma_{2A} = \sigma_{3A} = K_0\sigma_0, \quad \tau_{12A} = 0, \tag{3a}$$

where σ_3 denotes the out-of-plane stress, and the corresponding stress invariants

$$I_{1A} = (1 + 2K_0)\sigma_0, \qquad J_{2A} = \tfrac{1}{3}(1 - K_0)^2\,\sigma_0^2 \tag{3b}$$

To ensure initial elastic conditions, the following relationship between the stress invariants should hold:

$$\sqrt{J_{2A}} < \alpha I_{1A} \tag{4a}$$

that, through equation (3b), provides the following lower K_{0L} and upper K_{0U} limits of K_0 as functions of α:

$$K_{0L} = \frac{1 - \sqrt{3}\alpha}{1 + 2\sqrt{3}\alpha}, \qquad K_{0U} = \frac{1 + \sqrt{3}\alpha}{1 - 2\sqrt{3}\alpha} \tag{4b, c}$$

Copyright © 1999 John Wiley & Sons, Ltd.

As to the flow rule, it is defined by the plastic potential ψ which coincides with the yield function F (equation (2)) in case of associated behaviour, while it is expressed by the following function in the case of non associated behaviour with no plastic dilatancy:

$$\psi = \sqrt{J_2} \tag{5}$$

Starting from its initial state, the element is subjected to an increase of shear deformation γ_{12} that reaches the value γ_{12B} when the elastic limit (denoted by suffix B) is attained

$$\sigma_{1B} = \sigma_0, \quad \sigma_{2B} = \sigma_{3B} = K_0\sigma_0, \quad \tau_{12B} = G\gamma_{12B} \tag{6a}$$

$$I_{1B} = (1 + 2K_0)\sigma_0, \quad J_{2B} = \tfrac{1}{3}(1 - K_0)^2\sigma_0^2 + \tau_{12B}^2 \tag{6b}$$

Here G is the elastic shear modulus. The expression of τ_{12B}, and hence of γ_{12B}, is easily worked out by substituting equation (6b) into equation (2).

An increment $\dot{\gamma}_{12}$ of the shear strain beyond state B induces stress increments $\dot{\sigma}_3$ and $\dot{\tau}_{12}$ in the material element, and brings it to a plastic condition C:

$$\sigma_{1C} = \sigma_0, \quad \sigma_{2C} = K_0\sigma_0, \quad \sigma_{3C} = K_0\sigma_0 + \dot{\sigma}_3, \quad \tau_{12C} = \tau_{12B} + \dot{\tau}_{12} \tag{7}$$

The unknown stress increment $\dot{\tau}_{12}$ can be evaluated by imposing the following conditions, holding along the stress path from state B to C,

$$\mathrm{d}F = 0, \quad \dot{\varepsilon}_3 = 0, \quad \dot{\gamma}_{12} = \dot{\gamma}_{12}^{\mathrm{el}} + \dot{\gamma}_{12}^{\mathrm{pl}} \tag{8a–c}$$

where suffices 'el' and 'pl' denote, respectively, elastic and plastic components of strain.

The conditions (8) lead to the following system of differential equations:

$$\left(\frac{\partial F}{\partial \sigma_3}\right)_B \dot{\sigma}_3 + \left(\frac{\partial F}{\partial \tau_{12}}\right)_B \dot{\tau}_{12} = 0 \tag{9a}$$

$$\frac{\dot{\sigma}_3}{E} + \dot{\lambda}\left(\frac{\partial \psi}{\partial \sigma_3}\right)_B = 0 \tag{9b}$$

$$\dot{\gamma}_{12} = \frac{\dot{\tau}_{12}}{G} + \dot{\lambda}\left(\frac{\partial \psi}{\partial \tau_{12}}\right)_B \tag{9c}$$

In the above expressions, E is the Young modulus and $\dot{\lambda}$ is the increment of the plastic multiplier.

By eliminating $\dot{\lambda}$ and $\dot{\sigma}_3$ from equation (9), an incremental relationship can be established between $\dot{\tau}_{12}$ and $\dot{\gamma}_{12}$:

$$\dot{\tau}_{12} = D\dot{\gamma}_{12} \tag{10a}$$

where the coefficient D, which depends on the elastic and shear strength parametes (E, G, α) and on the initial stress state, through the coefficient K_0, has the following expression:

$$D = \frac{E(\partial F/\partial \sigma_3)_B(\partial \psi/\partial \sigma_3)_B}{E/G(\partial F/\partial \sigma_3)_B(\partial \psi/\partial \sigma_3)_B + (\partial F/\partial \tau_{12})_B(\partial \psi/\partial \tau_{12})_B} \tag{10b}$$

Now consider that softening takes place in the stress path from B to C if a positive strain increment $\dot{\gamma}_{12}$ induces a negative stress increment $\dot{\tau}_{12}$. In turn, this implies a negative value of coefficient D.

Copyright © 1999 John Wiley & Sons, Ltd.

This condition cannot occur in case of associated flow rule, i.e. when ψ and F coincide, since in this case D is always non-negative, and vanishes when (cf. equation (10b))

$$\left(\frac{\partial F}{\partial \sigma_3}\right)_{\mathrm{B}} = \left(\frac{\partial \psi}{\partial \sigma_3}\right)_{\mathrm{B}} = 0 \tag{11a}$$

i.e. when, taking into account equation (2),

$$K_0 = \frac{1 + 6\alpha^2}{1 - 12\alpha^2} \tag{11b}$$

In the above case, plastic flow takes place under constant stresses (cf. equations (9a) and (9b)).

In case of non-associated flow rule with no plastic dilatancy (equation (5)), the coefficient D might become negative. As an example, Figure 1 shows the variation of D within the limits of K_0 given by equations (4b) and (4c), for values of E and G corresponding to a Poisson ratio $\nu = 0{\cdot}25$ and for different values of α. It can be observed that, for any value of α, a range of K_0 exists in which D becomes negative and, therefore, softening may develop. In particular, the variation of D and of the stress increments $\dot{\sigma}_3$ and $\dot{\tau}_{12}$ with K_0 can be subdivided into the following three regions:

$$\text{if } K_{0\mathrm{L}} < K_0 \leqslant 1: \quad D \geqslant 0 \text{ and } \dot{\sigma}_3 \geqslant 0,\ \dot{\tau}_{12} \geqslant 0 \tag{12a}$$

$$\text{if } 1 < K_0 < \frac{1 + 6\alpha^2}{1 - 12\alpha^2}: \quad D < 0 \text{ and } \dot{\sigma}_3 < 0,\ \dot{\tau}_{12} < 0 \tag{12b}$$

$$\text{if } \frac{1 + 6\alpha^2}{1 - 12\alpha^2} \leqslant K_0 < K_{0\mathrm{U}}: \quad D \geqslant 0 \text{ and } \dot{\sigma}_3 \leqslant 0,\ \dot{\tau}_{12} \geqslant 0 \tag{12c}$$

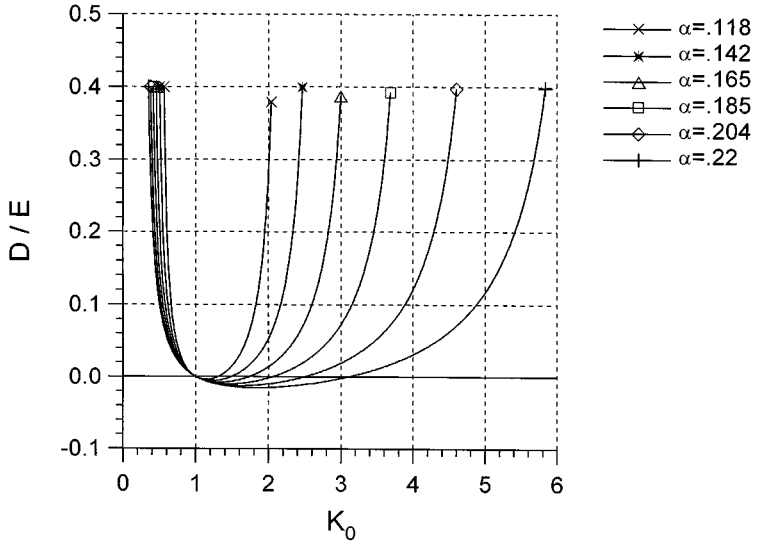

Figure 1. Variation of the D coefficient with K_0 (cf. equation (10b)) for different values of α

Copyright © 1999 John Wiley & Sons, Ltd.

Therefore, for a particular initial ratio between axial and lateral components of stress, it is possible to have a softening response, when $D < 0$, even with elastic perfectly plastic material, in case of a non-associated flow rule.

5. A NUMERICAL MODEL FOR SOFTENING PROBLEMS

The intrinsic and structural approaches mentioned in the previous sections represent different attempts to define the condition in which softening initiates. Based on this consideration, both approaches have been introduced in a finite element procedure applicable to the analysis of the formation and spreading of shear bands in stiff soils and weak rocks. In particular, the onset of localization is related to the loss of uniqueness of the solution of the non-associated elasto-plastic problem (structural softening) or to the attainment of a given limit of the non-reversible strains (material softening). When the chosen condition is fulfilled, the material in the localized zone undergoes a change of its structure, which leads to a local loss of its shear resistance. Hence, the frictional and cohesive shear strength parameters are gradually reduced in this zone, until reaching their residual values that characterise the so-called fully softened or ultimate state. During this process, the local elastic moduli of the material can be reduced as well.

5.1. Onset of softening

The material approach does not require particular comments, since it sees the loss of strength as a particular characteristic of the adopted stress–strain relationship. For instance, it can be assumed that softening initiates when a measure of the plastic strains, represented by their second invariant, reaches a given limit characterizing the material under examination.[9]

A more detailed description seems worthwhile for the structural approach. To this purpose, consider the system of differential equations governing the solution of a stress analysis problem for a given increment of external actions. From a mathematical standpoint, a bifurcation exists if the uniqueness of the solution of this system is lost or, in other words, if configurations different from the trivial one can be found at the end of the increment of external actions. When the uniqueness is lost the stability of each possible solution should be separately investigated.

According to the general theory of bifurcation, the described condition implies that the equations governing the variation between the expected and the alternative configuration lead to eigenvalue problem which admits non-trivial solutions.[10] The analysis of the associated eigenvectors defines the characteristics or 'mode' of each alternative solution. In this framework, the 'shear band analysis' seeks, as alternative configuration, the one describing a shear band mode of deformation.[53–56]

Let us consider now a plane strain problem, in a two-dimensional reference system x_1, x_2, concerning an unlimited, initially homogeneous, elastic perfectly plastic medium subjected to external actions that produced a continuous strain field within it.

Assume that under an increment of external actions the equations governing the stress analysis problem present multiple solutions characterized by a discontinuity in the strain field, or 'weak' discontinuity. A discontinuity of the displacement field, or 'strong' discontinuity,[57,58] would be in fact more appropriate in the case of fracturing.

This weak discontinuity, locally represented by a planar band in the **t** direction (Figure 2), can be described from a kinematic view point by the difference, or 'jump', $\Delta\dot{\mathbf{u}}$ between the

Copyright © 1999 John Wiley & Sons, Ltd.

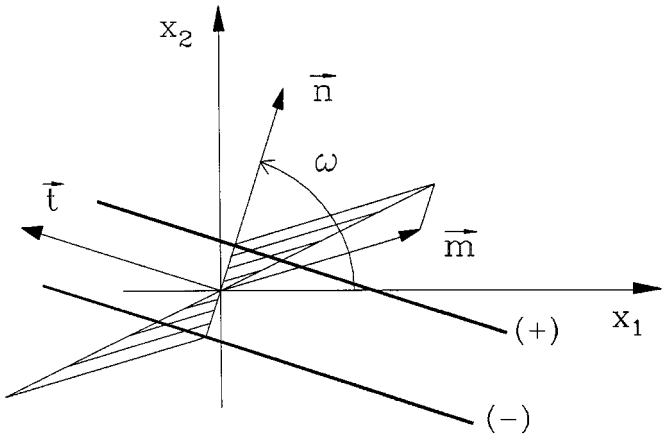

Figure 2. Plane of discontinuity in the strain field

displacement increments $\dot{\mathbf{u}}^+$ and $\dot{\mathbf{u}}^-$ at the band sides, which is assumed to vary linearly with the distance from the discontinuity itself:

$$\Delta\dot{\mathbf{u}} = \dot{\mathbf{u}}^+ - \dot{\mathbf{u}}^- = \dot{g}\mathbf{m}(\mathbf{n}^{\mathrm{T}}\mathbf{x}). \tag{13}$$

Here, $\mathbf{x}$ is the co-ordinate vector of the point where $\Delta\dot{\mathbf{u}}$ is evaluated, $\mathbf{n}$ is the unit vector normal to the discontinuity, $\mathbf{m}$ is the unit vector representing the displacement jump and $\dot{g}$ is its amplitude. Note that equation (13) considers both splitting ($\mathbf{m}$ parallel to $\mathbf{n}$) or shearing ($\mathbf{m}$ normal to $\mathbf{n}$) deformation modes, or combinations of them.

The jumps of the strain increments, obtained by deriving equation (13),

$$\Delta\dot{\varepsilon}_1 = \frac{\partial\Delta\dot{u}_1}{\partial x_1} = \dot{g}m_1n_1,\ \Delta\dot{\varepsilon}_2 = \frac{\partial\Delta\dot{u}_2}{\partial x_2} = \dot{g}m_2n_2,\ \Delta\dot{\gamma}_{12} = \frac{\partial\Delta\dot{u}_1}{\partial x_2} + \frac{\partial\Delta\dot{u}_2}{\partial x_1} = \dot{g}(m_1n_2 + m_2n_1) \tag{14}$$

can be expressed in the following matrix form, representing the condition of strain compatibility:

$$\Delta\dot{\boldsymbol{\varepsilon}} = [\Delta\dot{\varepsilon}_1\ \ \Delta\dot{\varepsilon}_2\ \ \Delta\dot{\gamma}_{12}\ \ \Delta\dot{\varepsilon}_3]^{\mathrm{T}} = \dot{g}\mathbf{N}\mathbf{m} \tag{15}$$

Here matrix $\mathbf{N}$ collects the direction cosines, n_1 and n_2, of the unit vector $\mathbf{n}$. Note that equation (15) also fulfils the compatibility condition across the strain discontinuity, i.e. $\Delta\dot{\varepsilon}_{\mathrm{t}} = 0$.

Now, assuming that after the onset of the discontinuity the same mechanical behaviour is followed by the material at the two band sides, the following relationship between the jumps of the stress and strain increments across the band can be written in terms of the tangent elasto-plastic constitutive matrix $\mathbf{D}^{\mathrm{ep}}$:

$$\Delta\dot{\boldsymbol{\sigma}} = \mathbf{D}^{\mathrm{ep}}\Delta\dot{\boldsymbol{\varepsilon}} \tag{16}$$

The case of bifurcation induced by a non symmetric $\mathbf{D}^{\mathrm{ep}}$ matrix, due to a non-associated flow rule, will be considered in the following. Note that bifurcation may occur also when different stress–strain paths, e.g. plastic loading and elastic unloading, take place at the two discontinuity

Copyright © 1999 John Wiley & Sons, Ltd.

sides.[59,60] It has been shown, however, that regardless the associativity of the flow rule this situation is less critical than the one characterized by the same stress–strain paths at the two sides. Hence, only the more critical condition is considered here.

The last condition to be imposed consists of the equilibrium equation, that requires the continuity of the increments of normal $\dot{\sigma}_n$ and shear $\dot{\tau}_{nt}$ stress across the band,

$$\Delta\dot{\sigma}_n = 0, \quad \Delta\dot{\tau}_{nt} = 0 \tag{17}$$

and that can be expressed in the following matrix form:

$$\mathbf{N}^T\Delta\dot{\boldsymbol{\sigma}} = \mathbf{0} \tag{18}$$

Finally, by substitution of compatibility (15) and constitutive (16) relationships within the equilibrium condition (18), the homogeneous system of governing equations is arrived at

$$\dot{g}(\mathbf{N}^T\mathbf{D}^{ep}\mathbf{N})\mathbf{m} = \mathbf{0} \tag{19}$$

Besides the trivial solution $\dot{g} = 0$, corresponding to a continuous strain field, the system (19) may admit also non-trivial solutions if

$$\det(\mathbf{N}^T\mathbf{D}^{ep}\mathbf{N}) = 0 \tag{20}$$

Equation (20) leads to a fourth-order polynomial equation, in the unknown direction cosines n_1 and n_2 (cf. Figure 2), which represents the condition of localization,

$$f(\omega) = a_0 n_1^4 + a_1 n_1^3 n_2 + a_2 n_1^2 n_2^2 + a_3 n_1 n_2^3 + a_4 n_2^4 = 0 \tag{21}$$

The coefficients a_i in the above equation are functions of the entries of matrix $\mathbf{D}^{ep}$. Therefore, for an elastic-perfectly plastic material with given yield and plastic potential functions, they depend solely on the material parameters, which are known, and on the current stress components. As a consequence, for such a kind of material it is possible to evaluate *a priori* the zones of the yield surface where equation (21) is fulfilled.

As an example, consider Drucker–Prager yield criterion

$$F = \sqrt{J_2} - \alpha I_1 - k = 0 \tag{22a}$$

with a non-associated flow rule depending on the following plastic potential ψ:

$$\psi = \sqrt{J_2} - \alpha^* I_1 - k^* = 0 \tag{22b}$$

In the non-associated case, the shear strength parameters k and α, which depend on cohesion and friction angle, do not coincide with the parameters k^* and α^* of the plastic potential ψ.

For this yield criterion, the Young modulus can be eliminated from all coefficients a_i in equation (21). In addition, these coefficients do not depend on the cohesive constant parameters k and k^*, since only the derivatives of F and ψ appear in matrix $\mathbf{D}^{ep}$. As a consequence, the locus of points fulfilling equation (21) depends solely on ν, α, α^* and it can be represented in the principal stress space by conical sectors of Drucker–Prager cone.[61] These are delimited by two generatrices, defined by particular values of Lode angle θ, which are symmetrical with respect to the out-of-plane stress axis σ_{III}. The intersection of these sectors with the deviatoric plane $I_1 = \text{const.}$ are shown in Figure 3 by heavy solid lines.

Copyright © 1999 John Wiley & Sons, Ltd.

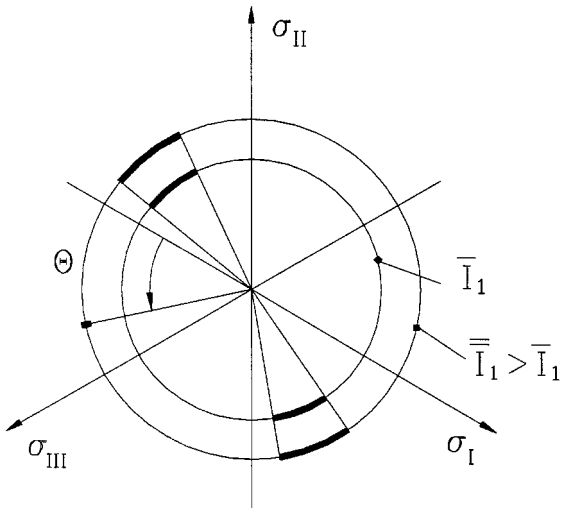

Figure 3. Intersections of the octahedral plane and the conical sectors representing the stress states fulfilling the condition of localization for Drucker–Prager yield criterion

If principal stress directions and reference axes coincide, the coefficients a_1 and a_3 vanish and equation (21) can be reduced to the following form:

$$f(\omega) = a_4 \operatorname{tg}^4 \omega + a_2 \operatorname{tg}^2 \omega + a_0 = 0 \tag{23}$$

where ω is the counterclockwise angle between axis x_1 and vector **n** (cf. Figure 2).

The characteristics of the solutions of equation (23) depend on the sign of coefficients a_0, a_2, a_4 and on the positiveness of its discriminant

$$d = a_2^2 - 4a_0a_4 \tag{24}$$

Figure 4 shows the variation of the discriminant (equation (24)) with Lode angle θ in the deviatoric plane. It can be observed that only two intervals of θ exist where the discriminant is positive. Their extension reduces with increasing α^* and vanishes when $\alpha^* = \alpha$, i.e. in case of associated flow rule.

Figure 5 reports the variation of coefficients a_0, a_2 and a_4 with θ, for different values of α, α^* and v. In particular, the diagrams indicate that a_2 is negative when the discriminant is positive while a_0 and a_4 are always positive. As a consequence, equation (23) in the real range admits always two positive and different solutions in terms of $\operatorname{tg}^2 \omega$, or four solutions in terms of $\operatorname{tg} \omega$, which are symmetrical with respect to the principal stress directions. It is also possible to show that two symmetrical solutions correspond to symmetrical directions **m** of the associated displacement jumps.[61]

A simple numerical example is discussed now, which illustrates the variation of the localization condition (equation (21)) with ω. The problem concerns the finite element analysis of a sample of elastic perfectly plastic, non-associated material (equations (22a) and (22b)) subjected to a plane strain compression test. The analysis is carried out by gradually increasing the vertical

Copyright © 1999 John Wiley & Sons, Ltd.

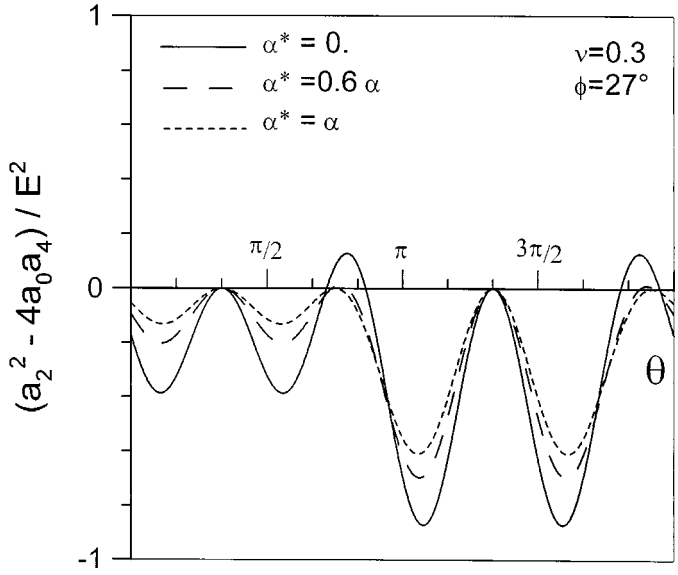

Figure 4. Variation of the discriminant of equation (23) with Lode angle θ for different values of the dilatancy parameter α^*

displacement of the upper loading base. Function (21) is evaluated at the integration points. The two limit cases of perfectly smooth and perfectly rough loading bases are considered in the calculations.

In the case of perfectly smoooth bases, the principal stress directions coincide with the reference axes and a uniform stress/strain state develops within the sample. Therefore, at each step of the analysis, the function $f(\omega)$ is constant throughout the sample. In addition, its value does not change in the elastic range, until the yield limit is attained. As soon as the yield condition is reached, $f(\omega)$ assumes the shape represented in Figure 6(a), characterized by two equal minima. The value of these minima decreases during loading, and bifurcation occurs when it vanishes. The four solutions of equation (21) reduce to two, which, due to the symmetry of the function with respect to $\omega = \pi/2$, are symmetrical with respect to the principal stress directions.

In the case of rough bases the stress/strain state is not uniform within the sample. As a consequence, bifurcation first occurs in its central part. In the subsequent steps of analysis the zone where equation (21) is fulfilled spreads along two symmetrical directions with respect to the vertical axis of the sample. Figure 6(b) shows the function $f(\omega)$ corresponding to an integration point close to the sample side. Note that the symmetry of the two solutions with respect to $\omega = \pi/2$ is lost. In fact, in this case the principal stress directions do not coincide with the reference system axes.

This example shows that the solutions of equation (21) reduce only to two values of ω and that a search of the minima of $f(\omega)$ is sufficient for verifying the condition of localization. In particular, bifurcation occurs at a given integration point when the corresponding minima vanish. Two symmetrical bands can show up at that point, the directions of which are defined by the two solutions ω.

Copyright © 1999 John Wiley & Sons, Ltd.

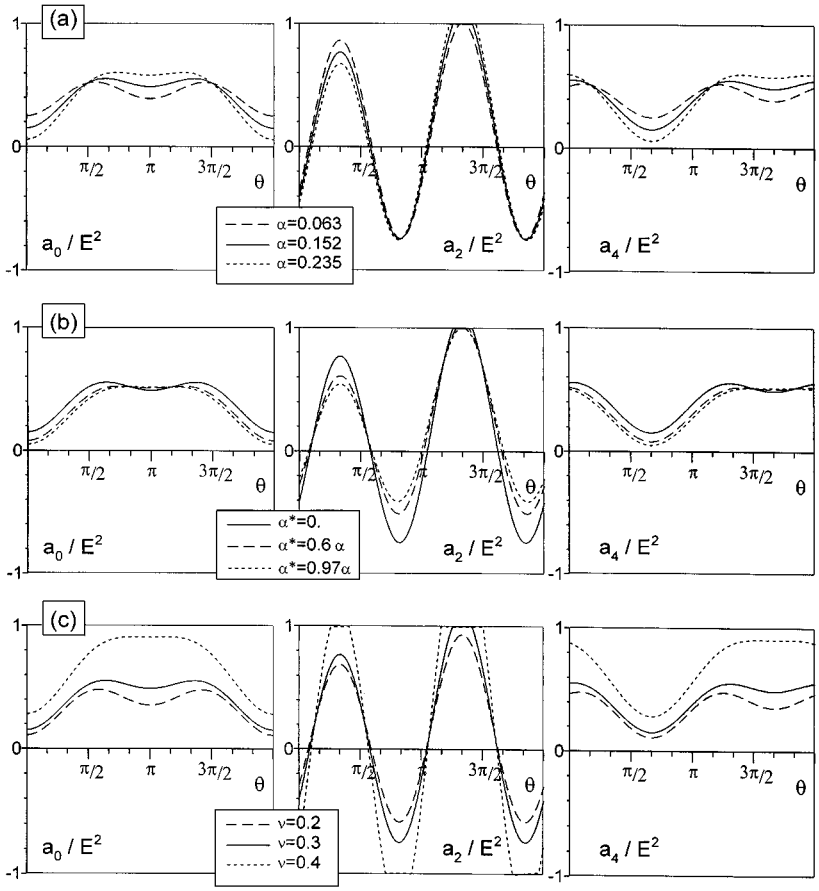

Figure 5. Variations of coefficients a_0, a_2 and a_4 with Lode angle θ for different values of the mechanical parameters: (a) α (with $\alpha^* = 0$, $\nu = 0.3$), (b) α^* (with $\alpha = 0.152$, $\nu = 0.3$) and (c) ν (with $\alpha = 0.152$, $\alpha^* = 0$)

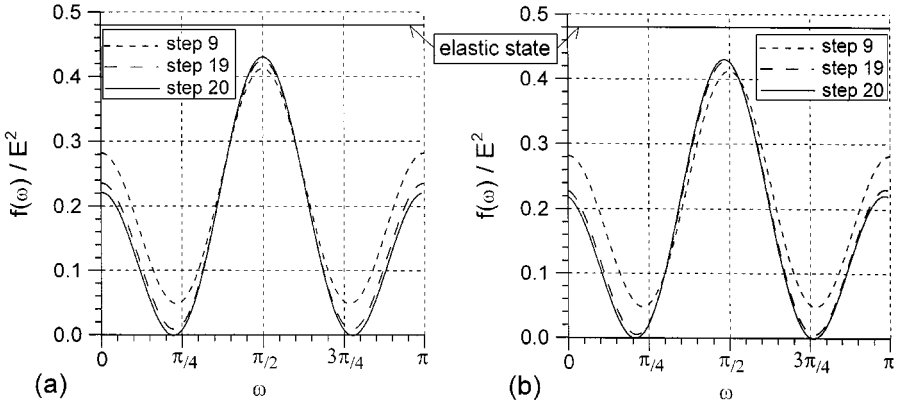

Figure 6. Function of localization (cf. equation (21)) for various steps of the numerical analysis of a compressed specimen with perfectly smooth (a) and perfectly rough (b) loading bases

Copyright © 1999 John Wiley & Sons, Ltd.

5.2. *Post-bifurcation path*

A post-bifurcation procedure is necessary to force the alternative path and to allow for the concentration of strains in the shear band. It should be considered that the occurrence of a strain discontinuity causes a change in the local structure of the material and a consequent loss of its shear resistance (and stiffness). This suggests to adopt a post bifurcation procedure in which the shear strength is reduced in the elements where the condition for softening initiation has been detected. This process is shared by both material and structural approaches.

It is assumed here that the parameters defining the shear resistance, e.g. cohesion and friction angle, keep their maximum values as long as the deformation is macroscopically homogeneous (peak condition), then gradually decrease while the plastic shear strains localize. Finally, they reach their minimum values when the shear band is fully developed (residual condition). In the calculations, a piecewise linear law (Figure 7) relates this progressive reduction to the increment of the plastic shear deformation γ^{d} with respect to its value at the onset of localization.

In addition, a particular provision is introduced to limit the expected mesh dependence of the solution. First, the parameter $\Delta\gamma^{\mathrm{d}}$ is calibrated on the basis of the available experimental data and of their simulation carried out on a chosen finite element grid. Then, when different grids are adopted, the previously determined parameter $\Delta\gamma^{\mathrm{d}}$ is modified depending on the difference between the size of the elements used for the parameter calibration and that adopted in the analysis.[43]

In fact, the reduction of shear resistance distributes the weakening effect of localization over a zone related to the area of the finite element. Actually, this effect should depend only on length and thickness of the shear band. The former is related to the element average size, while the latter depends on the material characteristics only. Hence, the parameter $\Delta\gamma^{\mathrm{d}}$ must be related to a one-dimensional 'measure' of the element. A relationship has been considered here that imposes a constant product between the parameter $\Delta\gamma^{\mathrm{d}}$ and the element mean size l. For instance, when modifying from element A to element B the following value $\Delta\gamma^{\mathrm{d}}_{\mathrm{B}}$ is adopted:

$$\Delta\gamma^{\mathrm{d}}_{\mathrm{B}} = \Delta\gamma^{\mathrm{d}}_{\mathrm{A}} \frac{l_{\mathrm{A}}}{l_{\mathrm{B}}} \tag{25}$$

The dependence of the solution on the discretization is effectively reduced by this provision. Only the dependence on the degrees of freedom remains, which is an intrinsic characteristic of the standard finite element method.

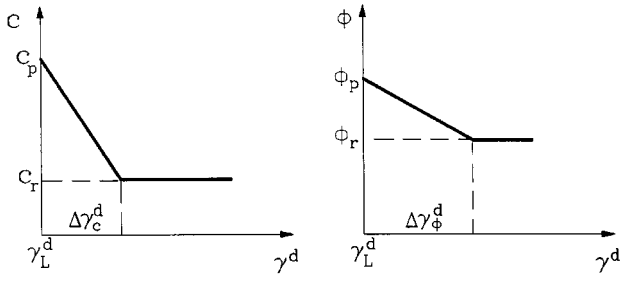

Figure 7. Law governing the reduction of the shear resistance parameters after the onset of localization

Copyright © 1999 John Wiley & Sons, Ltd.

5.3. *Computational aspects*

The above-described procedures have been implemented in the finite element code SoSIA2 (Soil–Structure Interaction Analysis) as a two-stage non-linear analysis.

The first stage corresponds to the check of the condition for softening initiation at each integration point at the end of each loading step.

According to the material approach, softening might occur when a given limit on the permanent shear deformation, characterising the material, is reached. This requires a simple test of a measure of the current plastic strain state, represented e.g. by its second invariant, against a corresponding parameter derived from the experimentally observed behaviour of the material.

If the structural approach is chosen, the test on localization requires the search of the minima of equation (21), whose coefficients are determined on the basis of the current state of stress. In principle, localization occurs when the two minima vanish. However, due to the finite size of the load increments, it is assumed that the localization condition is fulfilled when the minima reach a (small) negative value. The corresponding parameter γ_L^d (Figure 7) is determined as a measure of the current plastic strain state. Note that this parameter cannot vanish, since in the elastic state, equation (21) does not admit solutions.

It is worth observing that the choice of this condition has non-negligible consequences from the numerical standpoint. For instance, while the extension of the material approach to three-dimensional regime is rather straightforward, the same extension for the structural approach would involve appreciable difficulties and a substantial increase of the computational burden.

The second stage is activated only for the integration points where the localization condition has been fulfilled. Further load increments in general lead to increments of deviatoric plastic strains at these points. On their basis, the current values of the shear strength parameters are reduced according to the piecewise linear law previously described (Figure 7). Consequently, the current state of stress turns out to be no longer admissible with respect to the modified yield surface. Following the modified Newton–Raphson method, the stress state is brought back to the surface and its 'exceeding' portion is converted into equivalent nodal forces and applied as self-equilibrated external loads. An iterative process is then initiated, which terminates when no further variation of the shear strength parameters is observed for the current loading increment.

Note that the solution procedure for a given increment of external actions requires an iteration process consisting of a series of standard elasto-plastic analyses. In turn, the solution of each elasto-plastic analysis is based on a series of linear elastic calculations.

6. APPLICATIONS

The applicability potential of the proposed softening approach to actual geotechnical engineering problems is here discussed with reference to the stability analysis of underground openings. In particular, the numerical simulation of two series of laboratory tests is illustrated which were carried out on small-scale models of shallow tunnels. They aim at investigating the effects of strain localization on the stability, respectively, of the tunnel roof and of the excavation face.

Further aspects of the application of this strain softening approach, and in particular of the mentioned mesh dependence of the solution, have been presented elsewhere.[62]

Copyright © 1999 John Wiley & Sons, Ltd.

6.1. 2-Dimensional model

A first series of tests was performed at the Rock Mechanics Laboratory of Kobe University (Japan) on a plane strain model representing the cross section of a shallow, circular tunnel.[63] This small-scale model allows to study the condition of stability of the tunnel roof with the progress of excavation, which is simulated during the tests.

The medium surrounding the tunnel consists of an assembly of 5 cm long aluminium bars, having circular cross-section of diameter equal to 1·6 mm, for 85 per cent of the bars, and to 3 mm for the remaining 15 per cent. Depending on its relative density, the unit weight γ of the bar assembly ranges between 20·7 and 22·8 kN/m^3.

The model (Figure 8) consists of a 50 cm wide vertical rigid frame, containing two coaxial metal cylinders at its centre. They have diameter of 3·2 and 15 cm, respectively, and are connected by a front circular plate. The external cylinder provides a temporary support to the bars during their deposition. This is made by subsequent layers, slightly compacting each of them in order to obtain a fairly uniform distribution of relative density, approximately equal to 60 per cent ($\gamma = 21{\cdot}9$ kN/m^3). The deposition is completed when the overburden above the tunnel crown is equal to twice the tunnel diameter. The cylindrical bars ensure plane strain conditions during the tests, without need of a front wall. A 1 cm wide square grid, drawn on the frontal surface of the bar assembly, permits to measure the displacements induced during the test.

Four airbags, independently connected to a pressure source, are inserted within the gap between the two cylinders. The pressure of the airbags is raised to a value equivalent to the vertical pressure exerted by the bars at the tunnel crown (about 6·6 kPa) and the external cylinder is removed. The difference between the airbag pressure and the one acting on the rigid cylinder

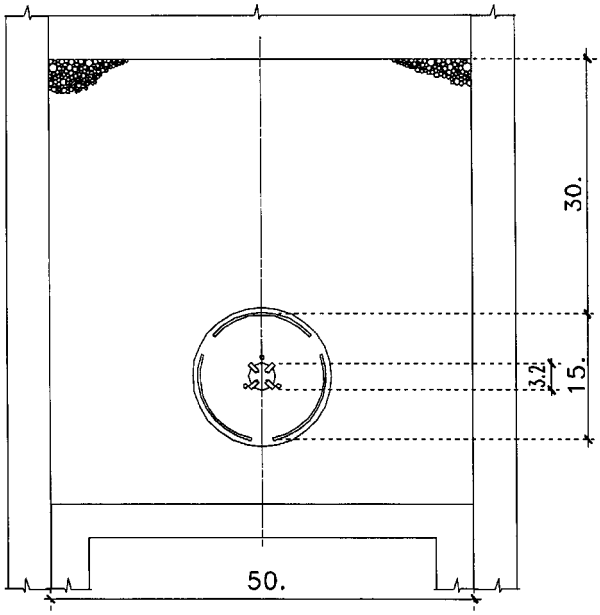

Figure 8. Tunnel model set-up (units: cm)

Copyright © 1999 John Wiley & Sons, Ltd.

does not induce appreciable displacements of the bars facing the opening during the cylinder removal.

At this stage of the test a first photograph of the front grid is taken which defines the initial position of each bar. Then the airbag pressure is decreased by steps of 50 Pa, simulating the tunnel excavation, until failure occurs. Photographs of the front grid are taken during this unloading process and subsequently digitized, from which displacement and strain distributions of the medium surrounding the opening are worked out.

The repeatability of the test was controlled by verifying that different tests performed under the same conditions led to sufficiently similar results.

Figure 9 shows the experimental set-up at the end of a test and the corresponding vertical displacements along horizontal lines at various depths. The strain localization initiates at the tunnel springlines and develops into two narrow shear bands. Failure of the tunnel occurs when the two bands form a collapse mechanism by reaching the ground surface.

The portion of the bar assembly contained between the two bands presents quite limited deformation and undergoes an almost rigid vertical settlement. The small lack of symmetry of this mechanism with respect to the tunnel centreline is likely to depend on local non-homogeneities of the initial relative density.

The experimental results indicate that the shear bands have an average thickness of about 3 cm, which corresponds to 16·5 times the mean diameter of the bars (1·8 mm). This is in agreement with the observations presented, e.g. by Roscoe[64] and by Muhlhaus and Vardoulakis.[18] It was also observed that the volume of material collapsed inside the opening is greater than that corresponding to the surface subsidence. This indicates an appreciable increase of the average void ratio during the test, which is related to the plastic dilatancy taking place, in particular, within the shear bands.

The mechanical characterization of the bar assembly, necessary for the numerical simulation of the model tests, was based on laterally constrained compression tests, for the evaluation of the elastic parameters, and on direct shear tests (Figure 10), for the evaluation of shear strength and dilatancy parameters. This experimental investigation led to the parameters listed in Table I. Here, subscripts p and r denote, respectively, peak and residual values; ϕ and ψ are friction and dilatancy angles; $\Delta\gamma^{d}$ is the increment of plastic shear strain from the beginning of localization to the attainment of the fully softened condition (cf. Figure 7).

The symmetry of the model tests with respect to the tunnel centreline permits to discretize only one-half of the whole problem.

The numerical results indicate that the localization condition is first fulfilled at the tunnel springline, when 35 per cent of excavation forces is reached. Subsequently, the zone of localization spreads almost steadily until reaching 74 per cent of total load. Then, further small increments of the applied forces lead to the formation of an almost vertical band that reaches the ground surface (Figure 11). The position of this band coincides with the zone where a sharp variation of vertical settlements was measured in the test and the softening effect leads to the actual localization of plastic shear strains within the same zone (Figure 12).

On the computed displacements the effect is shown by the sudden increase of the settlement rates of the tunnel crown and of the ground surface above it (Figure 13(a)), leading to the collapse of the opening. From a quantitative viewpoint, an acceptable agreement is observed between measured and computed settlements, cf. Figure 13(b). This indicates that the proposed numerical approach is able to reproduce, at least partially, the mechanism that develops around a tunnel driven into this kind of strain softening medium.

Copyright © 1999 John Wiley & Sons, Ltd.

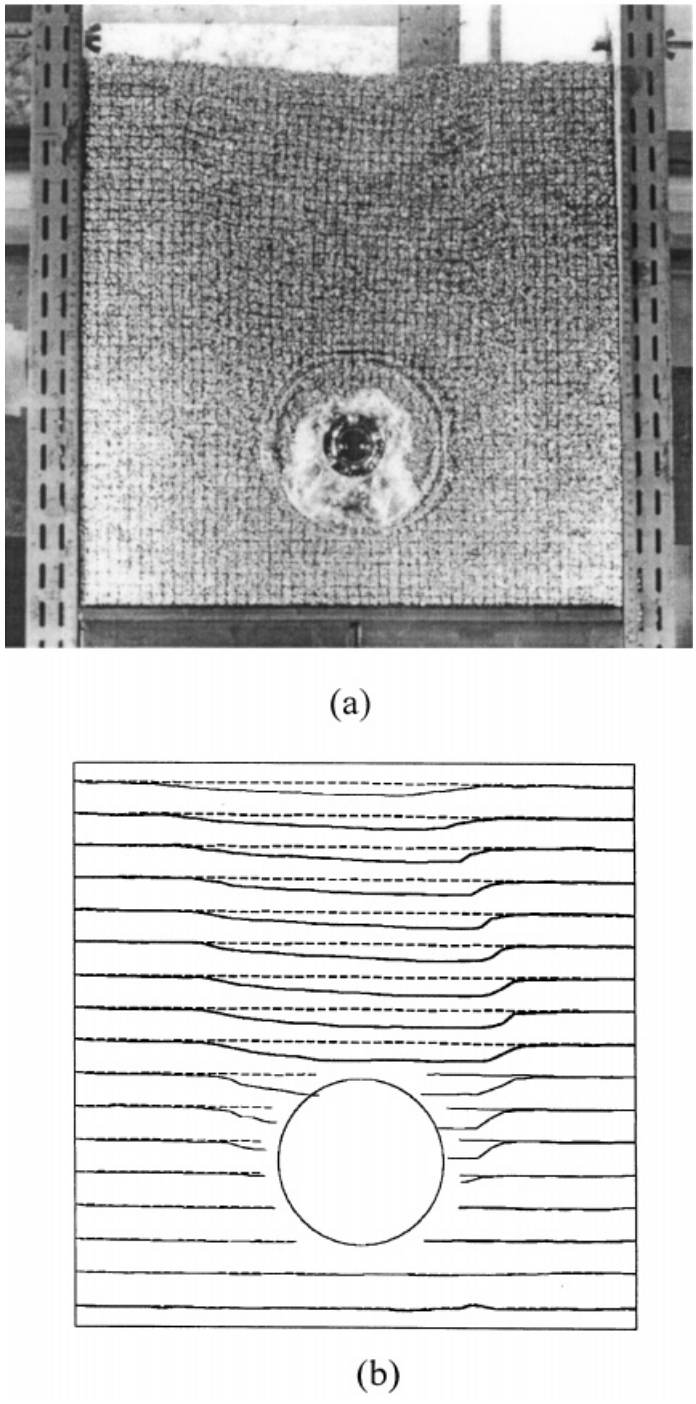

Figure 9. Bar assembly at failure (a) and corresponding digitized settlements along horizontal lines (b) (magn. factor = 1)

Copyright © 1999 John Wiley & Sons, Ltd.

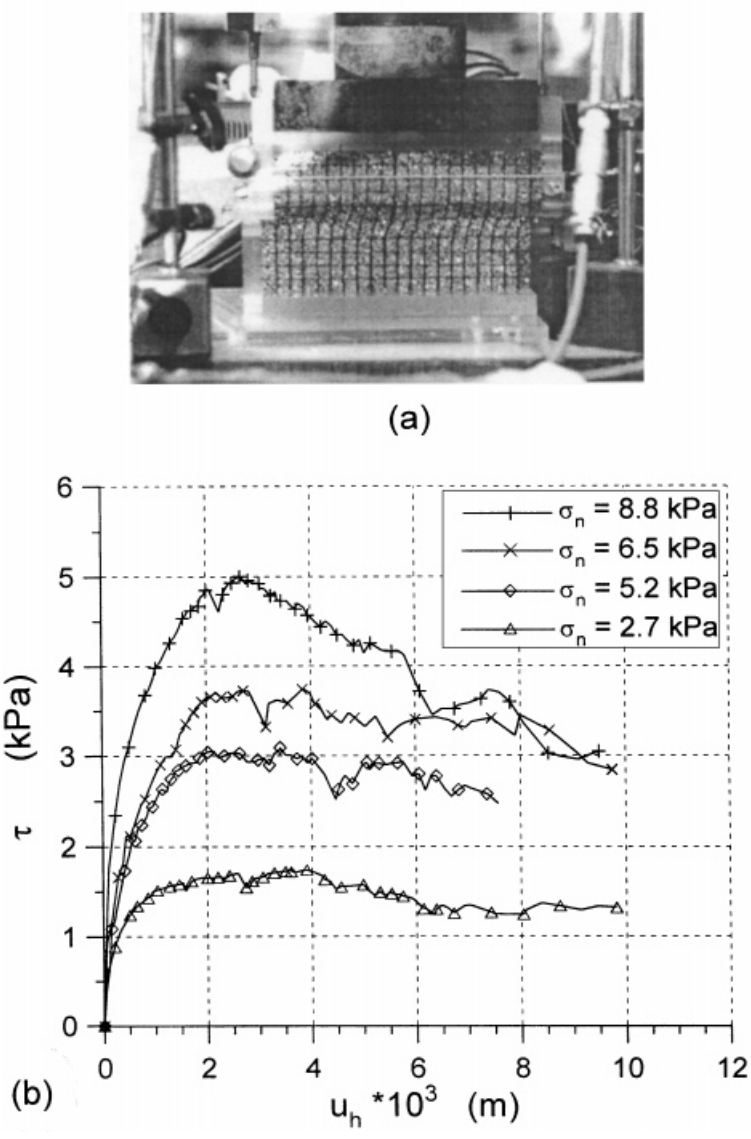

Figure 10. Direct shear test box for aluminium bar assembly (a) and test results for different values of the normal stress (b)

Table I. Constitutive parameters for the aluminium bar assembly

E (kPa)	v	γ (kN/m^3)	ϕ_p (deg)	ϕ_r (deg)	c	ψ_p (deg)	ψ_r (deg)	$\Delta\gamma^d$
3387	0·18	21·9	30·7	23·2	0	8·7	0	0·0025

Copyright © 1999 John Wiley & Sons, Ltd.

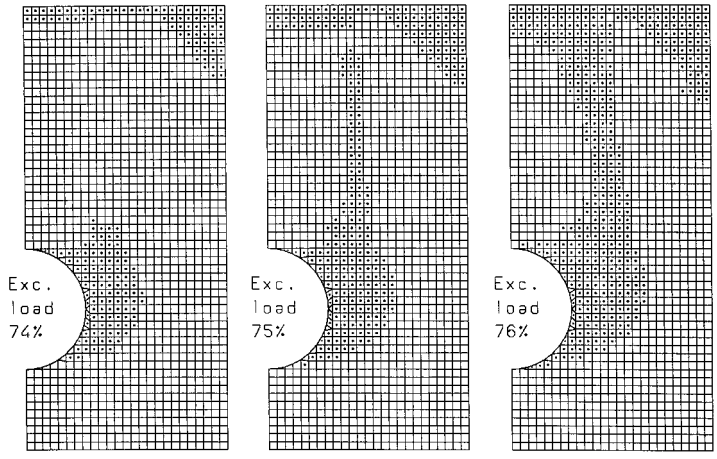

Figure 11. Spread of the zone where the condition of localization is fulfilled

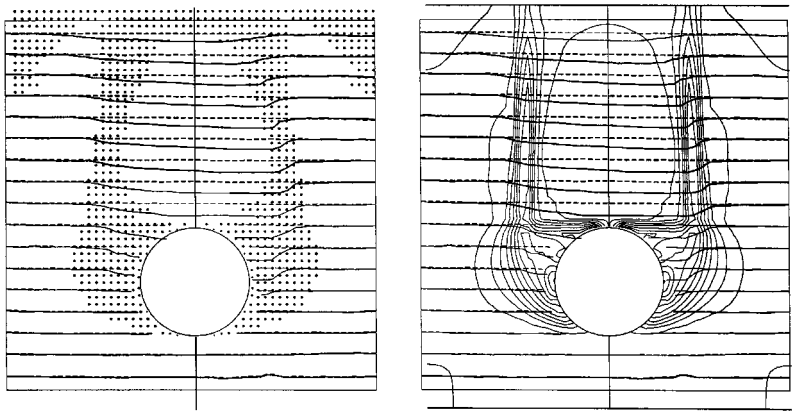

Figure 12. Overlapping of the measured settlements with the calculated zones of localization (left) and shear bands (right) (contour lines of the second invariant of deviatoric plastic strains, min = 0·2%, max = 4·2%, $\Delta = 0{\cdot}4\%$).

6.2. 3-Dimensional model

A second series of tests was performed at the Laboratories of Mitsubishi Heavy Industries in Takasago (Japan), on a 3-D model representing the portion of a shallow tunnel close to its face.[65] The stability of the excavation face is studied by decreasing the supporting pressure exerted on it by a vinyl airbag placed inside the tunnel (Figure 14(a)). Various measurements are taken during the unloading process, consisting of displacements and local values of the earth pressure. The dimensions of the model and the locations of the transducers are indicated in Figure 14(b).

The test preparation is similar to that described for the two-dimensional model. A natural sand was used in this case ($D_{50} = 0{\cdot}343$, $U_C = 2{\cdot}5$, $\gamma_g = 26{\cdot}6\ \mathrm{kN/m^3}$), with relative density ranging

Copyright © 1999 John Wiley & Sons, Ltd.

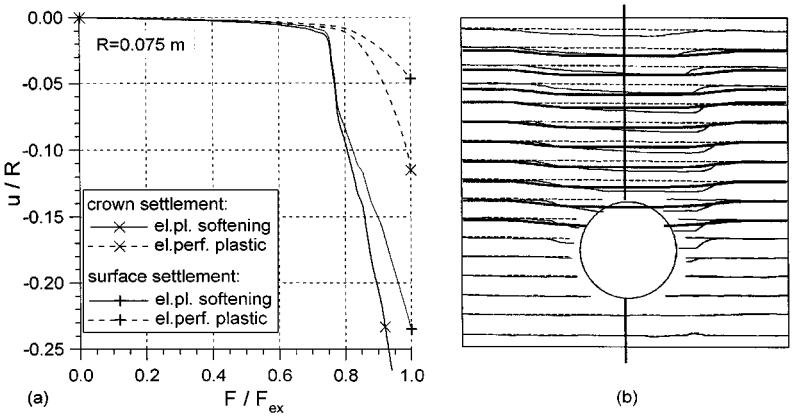

Figure 13. Variation of crown and surface settlements with the progress of excavation (a) and comparison between measured (thin line) and calculated (thick line) settlements along horizontal lines (b)

between 30 and 35 per cent and average unit weight of 14 kN/m^3. The sand is spread from a hopper and the model is gradually filled with layers of constant thickness. The stability of the tunnel face is ensured during deposition by increasing the pressure of the airbag. The displacements and pressure transducers are placed within the sand mass during its deposition and are connected to a digital data acquisition system. At the end of this process, the overburden above the tunnel crown coincides with the tunnel diameter.

The failure mechanism caused by the reduction of the airbag pressure consists of a cone of sand that moves towards the tunnel by sliding along a well defined bounding surface. Figure 15 shows the 'sinkhole' produced at the ground surface by this phenomenon.

The mechanical parameters of the sand, determined through conventional triaxial tests on saturated specimens, are summarized in Table II. Note that two values of the 'softening' parameter $\Delta\gamma^d$ are provided, that correspond to two different finite element grids used in the softening analyses.

The described model test was first simulated by a preliminary three-dimensional elastic perfectly plastic analysis. Figure 16 reports a comparison between measured and numerically evaluated settlements at various surface points (cf. Figure 14(b)). A fair agreement between the two sets of data exists only for points 'h3' and 'h6', that lie outside the zone where failure occurs. In fact, this zone is subjected to rather uniform settlements that are well reproduced even by a simple elastic perfectly plastic analysis. On the contrary, for the points inside the collapsed zone the agreement between numerical and experimental results is lost.

A second series of analyses, based on a two-dimensional, plane-strain discretization was performed with reference to the tunnel longitudinal section. A 'coarse' and a 'refined' grid were prepared for this purpose, the latter obtained from the former by subdividing its elements into four sub-elements. This required a correction of the softening parameter $\Delta\gamma^d$ that was changed from 0·001 to 0·002 (cf. equation (25)).

Even though a direct comparison between experimental and computed displacements is not possible in the case of two-dimensional analyses, a qualitative comparison between perfectly plastic and softening plane strain calculations still permits some interesting conclusions.

Copyright © 1999 John Wiley & Sons, Ltd.

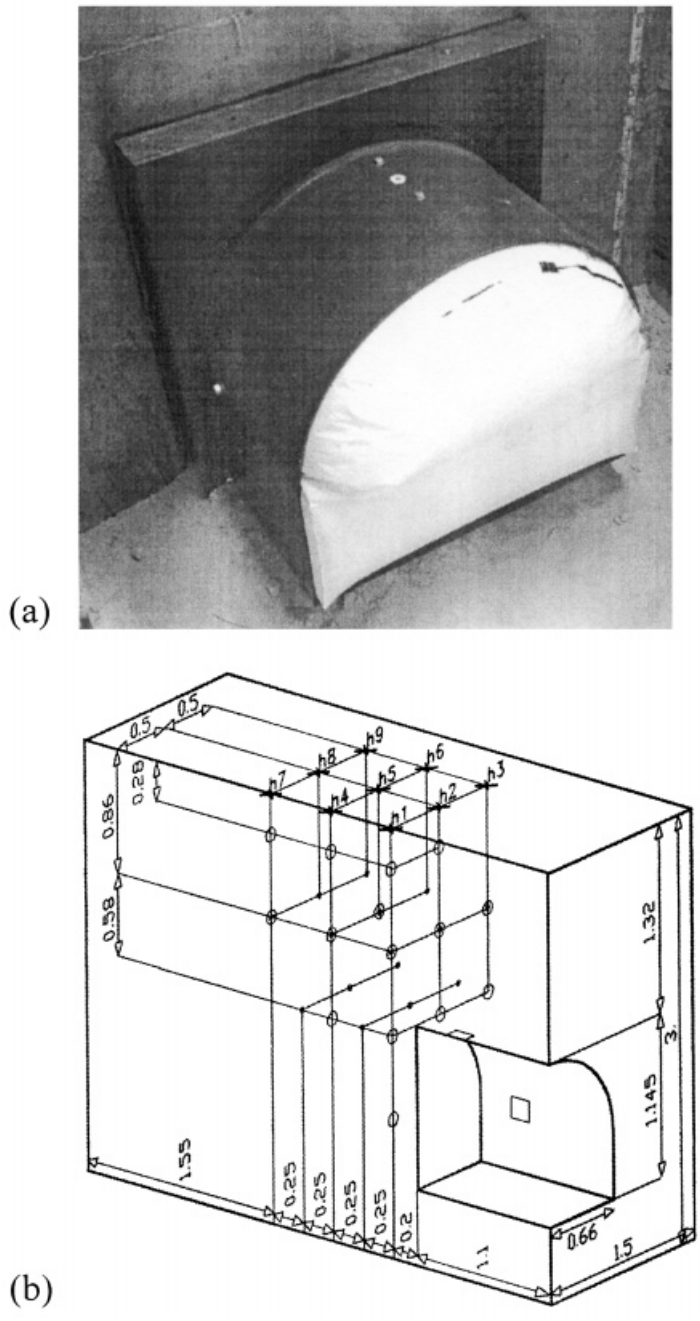

Figure 14. Tunnel lining with pressurized air bag (a) and axonometric view of one-half of the model with location of the transducers (b) (units: m)

Copyright © 1999 John Wiley & Sons, Ltd.

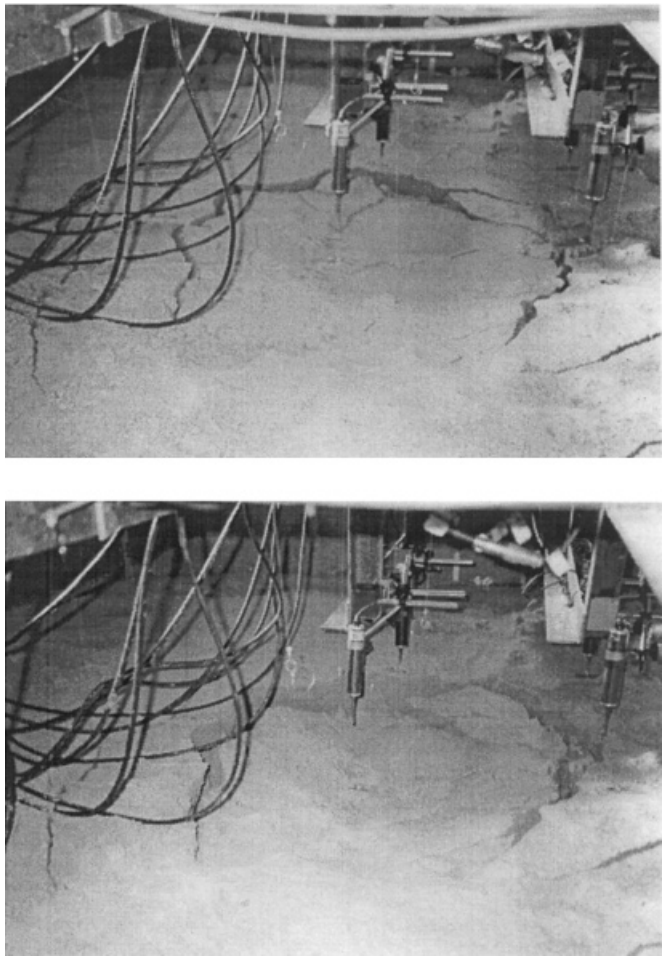

Figure 15. Observed ground surface at collapse during the final stages of the test

Table II. Constitutive parameters for the sand

E (kPa)	v	γ (kN/m^3)	ϕ_p (deg)	ϕ_r (deg)	c	ψ_p (deg)	ψ_r (deg)	$\Delta\gamma^d$
4220–12207	0·3	15·88	32	24	0	6·5	0	0·001–0·002

First, the effectiveness of the mentioned correction of parameter $\Delta\gamma^d$ can be assessed by comparing the loading-settlement curves of point 'h4' obtained from the two kinds of analysis (Figure 17). In fact, the discrepancy between the two softening analyses based on different grids is of the same order of magnitude of the one affecting the two corresponding elasto-plastic calculations.

Copyright © 1999 John Wiley & Sons, Ltd.

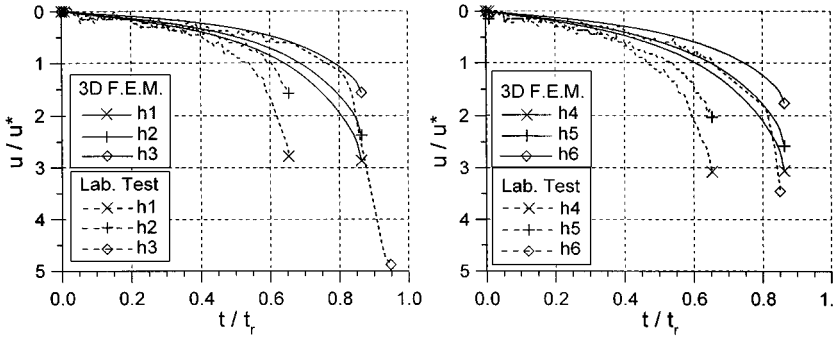

Figure 16. Variation of measured and calculated surface settlements with the progress of excavation. u^* is the maximum elastic settlement, t_r is the time of vanishing pressure

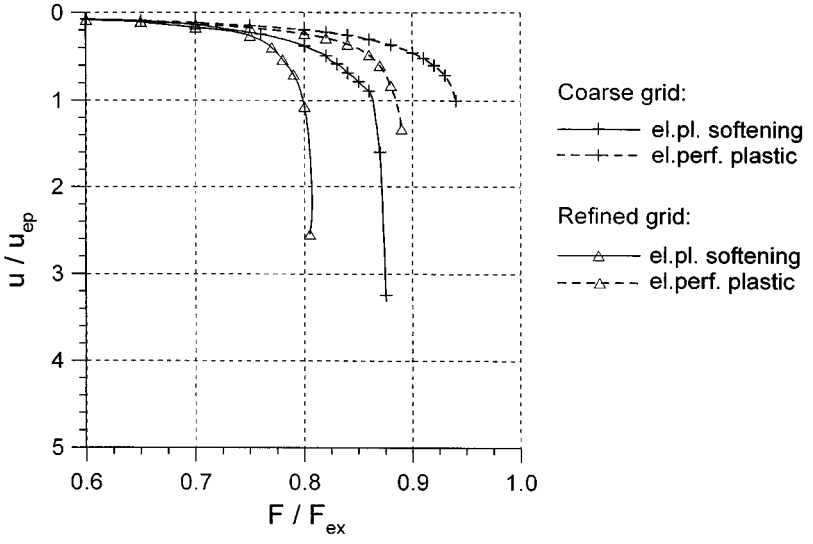

Figure 17. Variation of the settlement of surface point 'h4' with the progress of excavation for various analyses, u_{ep} is the maximum el.perf.plastic settlement obtained with coarse grid

The numerical results also point out the marked influence of strain softening on the overall behaviour of the medium surrounding the tunnel. In the softening analysis the localization condition is progressively fulfilled along the zones indicated in Figure 18 for two subsequent steps of the analysis. The strain concentration leads to the development of two shear bands that start from the tunnel crown and the invert arch and reach the ground surface. This effect is absent in the elastic perfectly plastic analysis where only a limited zone ahead of the tunnel face presents relatively high shear strains (Figure 19). This indicates that only the softening analysis provides some information about the development of the collapse mechanism and that its shape is in qualitative agreement with the experimental observation on the three-dimensional model.

Copyright © 1999 John Wiley & Sons, Ltd.

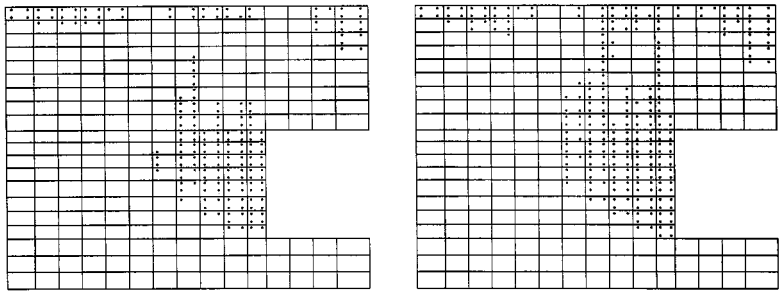

Figure 18. Spread of the zone where the condition of localization is fulfilled

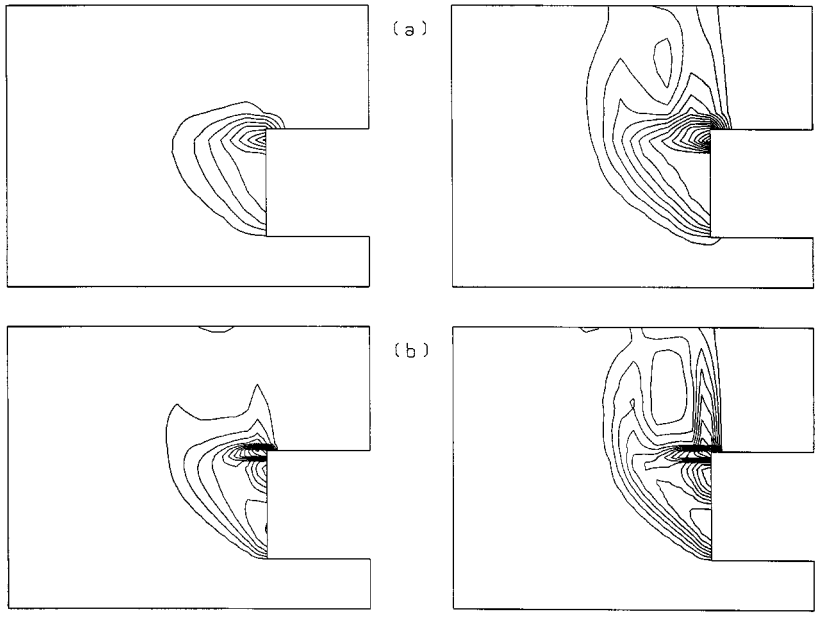

Figure 19. Shear bands at failure for el.perf. plastic (left) and el.pl. softening (right) analyses based on coarse (a) and refined (b) grids (contour lines of the second invariant of deviatoric plastic strains, min = 0·5%, Δ = 0·5%)

7. CONCLUSIONS

The study of the onset and development of shear bands has been here approached considering two main aspects of the phenomenon, referred to as 'structural' and 'material' softening.

The proposed numerical approach provides a reasonable estimation, at least from a qualitative viewpoint, of the behaviour experimentally observed. In particular, the numerical simulation of some laboratory tests of small-scale tunnel models led to an acceptable approximation of the collapse mechanism observed during the tests.

Copyright © 1999 John Wiley & Sons, Ltd.

Also a quantitative estimation of the global load–displacement diagrams could be attempted, provided that an accurate mechanical characterization of the material has been performed. In fact, any constitutive model involving strain softening generally results in a mechanical response, in terms of development of shear bands and consequent failure, which is highly sensitive to the accuracy of the material constants, such as those governing the loss of shear strength and, possibly, of stiffness.

It is worth noting that the proposed model is conceived as a relatively simple extension of a standard elasto-plastic non-associated model. The additional parameters required by this extension concern the loss of resistance due to shear band formation and, therefore, they should be determined by means of laboratory tests that allow for the development of such a phenomenon. In particular, it has been observed that plane strain compression tests[66] allow for a neater formation of shear bands than triaxial axisymmetric tests. Therefore, the plane strain device seems to be more suitable for the calibration of softening constitutive models than the standard triaxial apparatus.

ACKNOWLEDGEMENTS

This work summarizes the research carried out by the author to fulfil the requirements for the Ph.D. degree in Geotechnical Engineering at the Politecnico (Technical University) of Milan, Italy. The research was completed during a stage at the Division of Rock Mechanics of Kobe University, Japan. The guidance of A. Cividini, G. Gioda and S. Sakurai is gratefully acknowledged.

REFERENCES

1. K. Terzaghi, 'Stability of slopes of natural clay', *Proc. Int. Conf. Soil Mech. and Found Engng.*, Cambridge, MA, U.S.A. Vol. 1, 1936, pp. 161–165.
2. L. Bjerrum, 'Progressive failure in slopes of overconsolidated plastic clay and clay shales', *J. Soil Mech. Found Div. ASCE*, **93**(SM5), 1–49 (1967).
3. W. H. Hansmire and E. J. Cording, 'Soil tunnel test section: case history summary', *J. Geotech. Engng., ASCE*, **111**(11), 1301–1320 (1985).
4. P. A. Cundall, 'Numerical experiments on localization in frictional materials', *Ingenieur Archiv*, **59,** 148–159 (1989).
5. J. P. Bardet and J. Proubet, 'A numerical investigation of the structure of persistent shear bands in granular media', *Geotechnique*, **41,** 599–613 (1991).
6. R. J. Asaro and J. R. Rice, 'Strain localization in ductile single crystals', *J. Mech. Phys. Solids*, **25,** 309–338 (1977).
7. C. S. Desai, 'A consistent finite element technique for strain-softening behaviour', in J. Oden *et al.* (eds), *Proc. Int. Conf. Computational Meth. in Nonlin. Mech.*, Austin, TX 1974.
8. C. S. Desai, S. Somasundaram and G. Frantziskonis, 'A hierarchical approach for constitutive modelling of geologic materials', *Int. J. Numer. Anal. Meth. Geomech.*, **10,** 225–257 (1986).
9. A. Cividini and G. Gioda, 'Finite element analysis of direct shear tests of stiff clays', *Int. J. Numer. Anal. Meth. Geomech.*, **16,** 869–886 (1992).
10. R. Hill, 'A general theory of uniqueness and stability in elastic-plastic solids', *J. Mech. Phys. Solids*, **6,** 236–249 (1958).
11. Z. P. Bazant, T. Belytschko and T. P. Chang, 'Continuum theory for strain-softening', *J. Engng Mech. ASCE*, **110,** 1666–1692 (1984).
12. R. Larsson, K. Runesson and S. Sture, 'Finite element simulation of localized plastic deformation', *Arch. Appl. Mech.*, **61,** 305–317 (1991).
13. L. J. Sluys, 'Wave propagation, localisation and dispersion in softening solids,' *Ph.D. Thesis*, Technical University of Delft, The Netherlands, 1992.
14. H. E. Read and G. A. Hegemier, 'Strain softening of rock, soil and concrete—a review article', *Mech. Mater.* **3,** 271–294 (1984).
15. J. W. Rudnicki and J. R. Rice, 'Conditions for the localization of deformation in pressure-sensitive dilatant materials', *J. Mech. Phys. Solids*, **23,** 371–394 (1975).

Copyright © 1999 John Wiley & Sons, Ltd.

16. P. A. Vermeer, 'A simple shear band analysis usisng compliances', in P. A. Vermeer and H. Luger (eds), *Proc. IUTAM Conf. on Deformation and Failure of Granular Materials*, Balkema, Rotterdam, 1982, pp. 493–499.
17. R. De Borst, 'Bifurcations in finite element models with a non associated flow law', *Int. J. Numer. Anal. Meth. Geomech.*, **12,** 99–116 (1988).
18. H. B. Muhlhaus and I. Vardoulakis, 'The thickness of shear bands in granular materials', *Geotechnique*, **37,** 271–283 (1987).
19. J. Tejchman, 'Numerical study on localised deformation in a Cosserat continuum', in R. Chambon *et al.* (eds), *Proc. 3rd Int. Workshop on Localisation and Bifurcation Theory for Soils and Rocks*, Balkema, Rotterdam, 1993, pp. 257–274.
20. A. E. Groen and R. De Borst, 'Failure in plane strain compression using a non-associative Cosserat continuum', in A. Asaoka *et al.* (eds), *Proc. Int. Symp. Deformation and Progressive Failure in Geomechanics*, Elsevier Science, Oxford, 1997, pp. 39–44.
21. G. Pijaudier-Cabot and Z. P. Bazant, 'Nonlocal damage theory', *J. Engng Mech. ASCE*, **113,** 1512–1533 (1987).
22. P. A. Vermeer and R. B. Brinkgreve, 'A new effective non-local strain-measure for softening plasticity', in R. Chambon *et al.* (eds), *Proc. 3rd Int. Workshop on Localisation and Bifurcation Theory for Soils and Rocks*, Balkema, Rotterdam, 1993, pp. 89–100.
23. E. C. Aifantis, 'On the microstructural origin of certain inelastic models', *J. Mater. Engng Tech. ASME*, **106,** 326–330 (1984).
24. H. M. Zbib and E. C. Aifantis, 'On the localization and postlocalization behaviour of plastic deformations. I. On the initiation of shear bands', *Res. Mechanica*, **23,** 261–277 (1988).
25. H. M. Zbib and E. C. Aifantis, 'On the gradient-dependent theory of plasticity and shear banding', *Acta Mechanica*, **92,** 209–225 (1992).
26. I. Vardoulakis, E. C. Aifantis, 'Gradient dependent dilatancy and its implications in shear banding and liquefaction', *Ingenieur Archiv*, **59,** 197–208 (1989).
27. I. Vardoulakis, H. B. Muhlhaus and E. C. Aifantis, 'Continuum models for localized deformations in pressure sensitive materials', in G. Beer *et al.* (eds), *Proc. 7th Int. Conf. Computer Meth. and Adv. in Geomech.*, Balkema, Rotterdam, 1991, pp. 441–448.
28. H. B. Muhlhaus, R. De Borst and E. C. Aifantis, 'Constitutive models and numerical analyses for inelastic materials with micro-structure', in G. Beer *et al.* (eds), *Proc. 7th Conf. Computer Meth. and Adv. in Geomech*, Balkema, Rotterdam, 1991, pp. 377–385.
29. H. B. Muhlhaus and F. Oka, 'A gradient elasticity model for granular materials', in R. Chambon *et al.* (eds), *Proc. 3rd Int. Workshop on Localisation and Bifurcation Theory for Soils and Rocks*, Balkema, Rotterdam, 1993, pp. 201–209.
30. B. Loret and H. J. Prevost, 'Dynamic strain localization in elasto-(visco-)plastic solids, Part 1. General formulation and one-dimensional examples', *Comput. Meth. Appl. Mech. Engng.*, **83,** 247–273 (1990).
31. F. Oka, T. Adachi and A. Yashima, 'A strain localization analysis using a viscoplastic softening model for clay', *Int. J. Plasticity*, **11,** 523–545 (1995).
32. C. S. Desai, 'Constitutive modeling using the Disturbed State Concept as microstructure self-adjustment concept', in H. B. Muhlhaus (ed.), *Continuum Models for Materials with Microstructure*, Wiley, U.K., 1995.
33. C. S. Desai and J. Toth, 'Disturbed state constitutive modeling based on stress-strain and nondestructive behavior', *Int. J. Solids Struct.* **33,** 1619–1650 (1996).
34. C. S. Desai, C. Basaran and W. Zhang, 'Numerical algorithms and mesh dependence in the Disturbed State Concept', *Int. J. Numer. Meth. Engng.*, **40,** 3059–3083 (1997).
35. A. Needleman and V. Tvergaard, 'Finite element analysis of localization in plasticity', in J. T. Oden and G. F. Carey (eds), *Finite Element, Special Problems in Solid Mechanics*, Vol. 5, Prentice-Hall, New York, 1983, pp. 94–157.
36. M. Pastor, J. Peraire and O. C. Zienkiewicz, 'Adaptive remeshing for shear band localization problems', *Arch. Appl. Mech.*, **61,** 30–39 (1991).
37. O. C. Zienkiewicz, M. Huang and M. Pastor, 'Localization problems in plasticity using finite element with adaptive remeshing', *Int. J. Numer. Anal. Mech. Geomech.*, **19,** 127–148 (1995).
38. M. Ortiz, Y. Leroy and A. Needleman, 'A finite element method for localized failure analysis', *Comput. Meth. Appl. Mech. Engng* **61,** 189–214 (1987).
39. Y. Leroy and M. Ortiz, 'Finite element analysis of strain localization in frictional materials', *Int. J. Numer. Anal. Meth. Geomech.*, **13,** 53–74 (1989).
40. R. I. Borja and R. A. Regueiro, 'Finite element analysis of strain localization in excavations', in A. Asaoka *et al.* (eds), *Proc. Int. Symp. Deformation and Progressive Failure in Geomechanics*, Elsevier Science, Oxford, 1997, pp. 57–62.
41. T. Belytschko, J. Fish and E. Engelmann, 'A finite element with embedded localization zones', *Comput. Meth. Appl. Mech. Engng*, **70,** 59–89 (1988).
42. J. Fish and T. Belytschko, 'A finite element with a unidirectionally enriched strain field for localization analysis', *Comput. Meth. Appl. Mech. Engng.*, **78,** 181–200 (1990).
43. S. Pietruszczak and Z. Mroz, 'Finite element analysis of deformation of strain-softening materials', *Int. J. Numer. Meth. Engng.*, **17,** 327–334 (1981).
44. S. Pietruszczak and X. Niu, 'On the description of localized deformation', *Int. J. Numer. Anal. Meth. Geomech.*, **17,** 791–805 (1993).

Copyright © 1999 John Wiley & Sons, Ltd.

45. H. F. Schweiger, M. Karstunen and N. G. Pande, 'Modelling strain localization in soils using multilaminate model and homogenisation technique', in A. Asaoka *et al.* (eds), *Proc. Int. Symp. Deformation and Progressive Failure in Geomechanics*, Elsevier Science, Oxford, 1997, pp. 97–102.
46. D. A. Shuttle and I. M. Smith, 'Numerical simulation of shear band formation in soils', *Int. J. Numer. Anal. Meth. Geomech.*, **12,** 611–626 (1988).
47. A. H. C. Chan, L. Jendele, D. Muir Wood and A. Drescher, 'Numerical analyses of strain localization using randomly distributed material properties', in G. N. Pande and S. Pietruszczak (eds), *Proc. 4th Int. Symp. Numer. Mod. in Geomech*, Balkema, Rotterdam, 1992, pp. 349–355.
48. R. De Borst, L. J. Sluys, H. B. Muhlhaus and J. Pamin, 'Fundamental issues in finite element analyses of localization of deformation', *Engng Comput*. **10,** 99–121 (1993).
49. R. Chambon, J. Desrues and I. Vardoulakis (eds), *Localisation and bifurcation theory for soils and rocks*, *Proc. 3rd Int. Workshop*, Grenoble, Balkema, Rotterdam, 1993.
50. Y. Tomita, 'Simulation of plastic instabilities in solid mechanics', *Appl. Mech. Rev. ASME*, **47,** 171–205 (1994).
51. I. Vardoulakis and J. Sulem, *Bifurcation Analysis in Geomechanics*, Chapman & Hall, Glasgow, 1995.
52. A. Asaoka, T. Adachi and F. Oka (eds), *Deformation and progressive failure in geomechanics*, *Proc. Int. Symp.*, Nagoya, Elsevier Science, Oxford, 1997.
53. T. Y. Thomas, *Plastic Flow and Fracture in Solids*, Academic Press, New York, 1961.
54. R. Hill and J. W. Hutchinson, 'Bifurcation phenomena in plane tension test', *J. Mech. Phys. Solids*, **23,** 239–264 (1975).
55. J. R. Rice, 'The localization of plastic deformation', in W. T. Koiter (ed), *Proc. 14th Int. Conf. on Theoretical and Applied Mechanics*, Delft, North-Holland, Amsterdam, 1976.
56. A. Needleman, 'Non-normality and bifurcation in plane strain tension and compression', *J. Mech. Phys. Solids*, **27,** 231–254 (1979).
57. N. S. Ottosen and K. Runesson, 'Properties of discontinuous bifurcation solutions in elasto-plasticity', *Int. J. Solids Struct.* **27,** 401–421 (1991).
58. R. Larsson, K. Runesson and K. Axelsson, 'Localization properties of a frictional material model based on regularized strong discontinuity', *Int. J. Numer. Anal. Math. Geomech.*, **20,** 771–783 (1996).
59. J. R. Rice and J. W. Rudnicki, 'A note on some features of the theory of the localization of deformation', *Int. J. Solids Struct.* **16,** 597–605 (1980).
60. J. Desrues and R. Chambon, 'Shear band analysis for granular materials: the question of incremental non-linearity', *Ingenieur Archiv*, **59,** 187–196 (1989).
61. D. Sterpi, 'Influence of the strain localization phenomenon on the stability of underground openings', *Ph.D. Thesis*, Technical University of Milano, Italy, 1997 (in Italian).
62. D. Sterpi, A. Cividini and M. Donelli, 'Numerical analysis of a shallow excavation in strain softening rock', in T. Fujii (ed), *Proc. 8th Int. Congr. on Rock Mechanics*, Balkema, Rotterdam, Vol. 2, 1995, pp. 545–549.
63. S. Akutagawa, K. Ogawa and S. Sakurai, 'An analytical and experimental investigation on stability of underground openings', in J. X. Yuan (ed.), *Proc. 9th Int. Conf. Computer Meth. and Adv. in Geomech.*, Balkema, Rotterdam, 1997, pp. 1495–1500.
64. K. H. Roscoe, 'The influence of strains in soil mechanics', *Geotechnique*, **20,** 129–170 (1970).
65. D. Sterpi, A. Cividini, S. Sakurai and S. Nishitake, 'Laboratory model tests and numerical analysis of shallow tunnels', in G. Barla (ed.), *Proc. Int. Symp. Eurock'96*, Balkema, Rotterdam, 1996, pp. 689–696.
66. I. G. Vardoulakis and A. Drescher, 'Development of biaxial apparatus for testing frictional and cohesive granular media', *Final Report to the National Science Foundation*, *NSF Grant no. CEE* 84-06500, University of Minnesota, U.S.A., 1988.

Copyright © 1999 John Wiley & Sons, Ltd.